processes

MDPI

Article

Effect of the Mixer Design Parameters on the Performance of a Twin Paddle Blender: A DEM Study

Behrooz Jadidi, Mohammadreza Ebrahimi, Farhad Ein-Mozaffari * and Ali Lohi

Department of Chemical Engineering, Toronto Metropolitan University, 350 Victoria Street, Toronto, ON M5B 2K3, Canada
* Correspondence: fmozaffa@torontomu.ca

Abstract: The design parameters of a mixing system have a major impact on the quality of the final product. Therefore, identifying the optimum parameters of mixing systems is highly relevant to various industrial processes dealing with particulate flows. However, the studies on the influences of the mixer's design features are still insufficient. In this study, the Discrete Element Method (DEM) is used to examine the impact of paddle angle, width, and gap on the mixing performance of a twin paddle blender. The mixing performance and particle flow are assessed using the relative standard deviation (RSD) mixing index, velocity field, diffusivity coefficient, granular temperature, the force acting on particles, and the mixer's power consumption. The mixing performance is highest for a paddle angle of 0° at the cost of the highest forces acting on particles. The paddle width is indicated as a critical factor for achieving better mixing quality. In contrast, the powder mixing efficiency and the mixer's power consumption are not significantly affected by the paddle gap. The results regarding the power consumption denote that the mixer using the paddle angle of 60° has the minimum power consumption. Moreover, increasing the paddle width results in the enhancement of the mixer's power consumption.

Keywords: particle mixing; twin paddle blender; batch mixing; Discrete Element Method (DEM); impeller design

Citation: Jadidi, B.; Ebrahimi, M.; Ein-Mozaffari, F.; Lohi, A. Effect of the Mixer Design Parameters on the Performance of a Twin Paddle Blender: A DEM Study. *Processes* **2023**, *11*, 733. https://doi.org/10.3390/pr11030733

Academic Editor: Kejun Dong

Received: 25 January 2023
Revised: 20 February 2023
Accepted: 27 February 2023
Published: 1 March 2023

1. Introduction

Mixing and particulate processing are carried out in various manufacturing industries, including chemical, cosmetics, food, and pharmaceuticals [1,2]. Optimizing the performance of a mixer is a critical task for industries dealing with particle processing. Achieving higher product homogeneity in a shorter time is usually the main goal of mixer performance optimization. Insufficient mixing can cause the final product to be rejected due to poor quality. It is generally possible to enhance a mixer's performance by altering its design [2] or adjusting operational parameters [3,4].

It is vital to closely monitor the changes in power consumption and stress experienced by particles at each condition when manipulating the operational parameters or design variables of a mixing system to identify the optimum conditions. For instance, increasing the mixer's rotational speed in most cases leads to shortening the mixing time, but simultaneously, it could also increase the stress acting on particles, which may lead to particle breakage for brittle materials [2]. Therefore, a detailed analysis of mixing performance (usually quantified by the RSD mixing index), power consumption, and stress analysis need to be conducted when trying to optimize the mixing system performance for a specific process.

Various manufacturing processes employ mixers equipped with mechanical impellers (agitators) [2,5]. This group of mixers (convective mixers) consists of single/double stationary vessels and a rotating blade(s) or impeller(s). The impeller moves through the bed of particles and mixes them. Convective mixers can be classified according to the shape

of their impellers, including ribbon, plow, paddle, and screw blenders. There are several studies in the literature analyzing the efficiency of these mixers using experiments and numerical simulations, both qualitatively and quantitatively [2–4,6,7].

The Discrete Element Method (DEM) approach, initially introduced by Cundall and Strack [8], is the most common numerical technique used to analyze the behavior of granular materials in mixing systems [9,10]. The method provides particle-level information that is currently impossible or very difficult to measure experimentally (e.gs., the forces acting on each particle individually as well as particles' positions and velocities).

In several research studies on various agitated blenders, the effect of operating parameters (e.g., RPM, vessel fill level, loading arrangement) on the mixing performance was assessed using both experiments and DEM simulations [3,4,7,11–13]. Impeller configuration/design is another decisive parameter that affects the mixing quality in a convective mixer [14]. The amount of momentum imparted to the particle bed is generally determined by the agitator design, which directly affects the particle flow pattern and the mixing efficiency of powder blenders [2]. Furthermore, the impeller design can also enhance or reduce segregation in a mixing system containing a polydisperse particle mixture. Therefore, the design and development of an optimal agitated mixer greatly depend on the understanding of the effect of impeller configuration on mixing [2]. Despite the significant role of the impeller design on mixing performance, only a few studies in the literature have reported its impact on the mixing process in an agitated mixer. For example, Chandratilleke et al. [15] and Siraj et al. [16,17] used DEM to study the effects of the blade's shape and angle on particulate flow behavior in a system equipped with a single blade containing a bed of binary mixture. They found that both forces that are acting on the blade and interparticle forces decreased by increasing the blade angle. Daraio et al. [18] explored the effect of impeller arm length on particulate flow quality in a vertically stirred mill consisting of spherical particles. Calculating velocity, collision frequency, energy dissipation, and hydrostatic pressure from their DEM simulations, the authors concluded that the long-arm impeller design was the most effective in shortening the mixing time and enhancing the particle bed agitation. In order to assess the ribbon design effect on mixer performance, Jin et al. [19] analyzed the mixing rate, particles' path line, velocity distribution, and forces acting on particles for three different impeller designs using both DEM and experimental investigation. It was found that the impeller (ribbon) design significantly affected the mixing performance. In another research, Tsugeno et al. [20] studied the impacts of blade width and blade pitch on the particle mixing quality in a ribbon blender. The results revealed that the mixing efficiency, quantified by mixing progress per one paddle rotation, improved noticeably when the blade width was increased. On the other hand, the blade pitch did not affect the mixing efficiency significantly. Therefore, the blade width was identified as a critical design parameter to enhance ribbon mixer performance.

Ebrahimi et al. [2] used DEM to examine the mixing efficiency of a single paddle mixer as a function of impeller design. Five different impeller configurations were examined, and by calculating RSD, the force acting on particles, diffusion coefficient, Peclet number, and granular temperature, the authors demonstrated that the impeller configurations significantly affected mixing performance and granular behavior. Chandratilleke et al. [21] used DEM to explore the influences of blade rake angle and gap on powder mixing in a cylindrical bladed blender. The simulation results demonstrated that the blade with a 90° rake angle achieved the maximum mixing rate with the cost of the highest inter-particle forces. In contrast, a blade with a rake angle of 135° produced the slowest mixing rate when the inter-particle stresses were minimum.

Boonokanokwong et al. [22] studied the influence of the number of impeller blades on mixing kinetics and particulate flow in a bladed mixer. The RSD and Lacey mixing index values were calculated for various mixer designs. The results revealed that mixing systems equipped with two or three impeller blades had superior mixing efficiency compared to mixing systems with one or four blades. Particle diffusivity and granular temperature were also higher in the two- and three-bladed mixers than in the one- and four-bladed mixers.

It is noticeable that in all the studies summarized above, the influence of the impeller design on the mixing performance of laboratory-scale single-vessel mixers has been analyzed. In this study, however, we use the DEM method to study the effect of the impeller configuration (blade's gap, width, and angle) on the mixing quality of a large-scale double paddle blender, which has not been reported in the literature previously. In order to achieve the research's objectives, particle velocity, mixing kinetics, granular temperature, particle diffusivity, forces acting on particles, power consumption, and impeller torque were calculated using the DEM simulations. The RSD mixing index was also calculated to evaluate the mixing degree. In this study, all the simulations were carried out with a constant impeller rotational speed (40 RPM), fill level (40%), and top-bottom loading arrangement. These operational conditions were selected based on our previous studies on this double-paddle blender [3]. Following is the outline of the present paper: Section 2 discusses the DEM model, the geometry configurations, and the characterization methods used in this study. Section 3 discusses the results, including the effects of the impeller configurations on the mixing performance, mixing kinetics, particle diffusivity, forces acting on particles, and the mixer power consumption. Finally, the last section (Section 4) concludes the paper.

2. Modelling and Simulations

In order to determine the position, velocity, and acceleration of each particle in the mixer, the Discrete Element Method (DEM) approach is employed in our study. In this method, the collision dynamics of particles are modeled during the mixing process. The DEM approach and the simulation conditions are presented in this section, followed by the descriptions of mixing characterization methods used in the current research.

2.1. Discrete Element Method (DEM)

Newton's equations of motion are solved to calculate the velocity of each particle over time. For small time steps, it can be assumed that the gravitational force and direct collisions with other particles are the only factors affecting the dynamics of the particles. Using The DEM method, particles' positions, velocities as well as forces acting on particles can be obtained. In the present study, in order to calculate the normal and tangential forces, the Hertz–Mindlin contact model is employed [3]. The torque and contact force expressions can be found in our previous publications and literature [3,6,23], and for brevity, those equations are not presented in this study. LIGGGHTS (DCS, Linz, Austria), an open-source DEM package, is utilized for all the simulations reported in the current study [23].

It has been widely verified that the DEM is reliable in many numerical simulations of particle mixing in the paddle mixers [13,24–27]. However, prior to starting the simulation runs, the DEM model needs to be validated. It should be mentioned that the DEM model utilized in this paper has been validated in our previous study against experimental data obtained from a rotary drum [3]. Consequently, the physical properties employed in the simulations can be found in our previous study [3], and for concision, they are not reiterated in this study.

2.2. Simulation Conditions

2.2.1. Geometry of the Mixer

The mixer investigated in this study is the same as the mixer analyzed in our previous studies [3,13,28]. For brevity, the dimensions of the mixer used in this study are not provided in this paper. However, a detailed description of the mixer's specifications can be found in our previous publication [3]. Briefly, the double paddle blender consists of two cylindrical vessels with two identical impellers arranged alternately at 90°. In this article, the coordinate system's origin is placed at the center of the intersection of two cylindrical-shaped vessels. Figures 1 and 2 illustrate the vessel geometry and impeller geometry (used in our base case simulation).

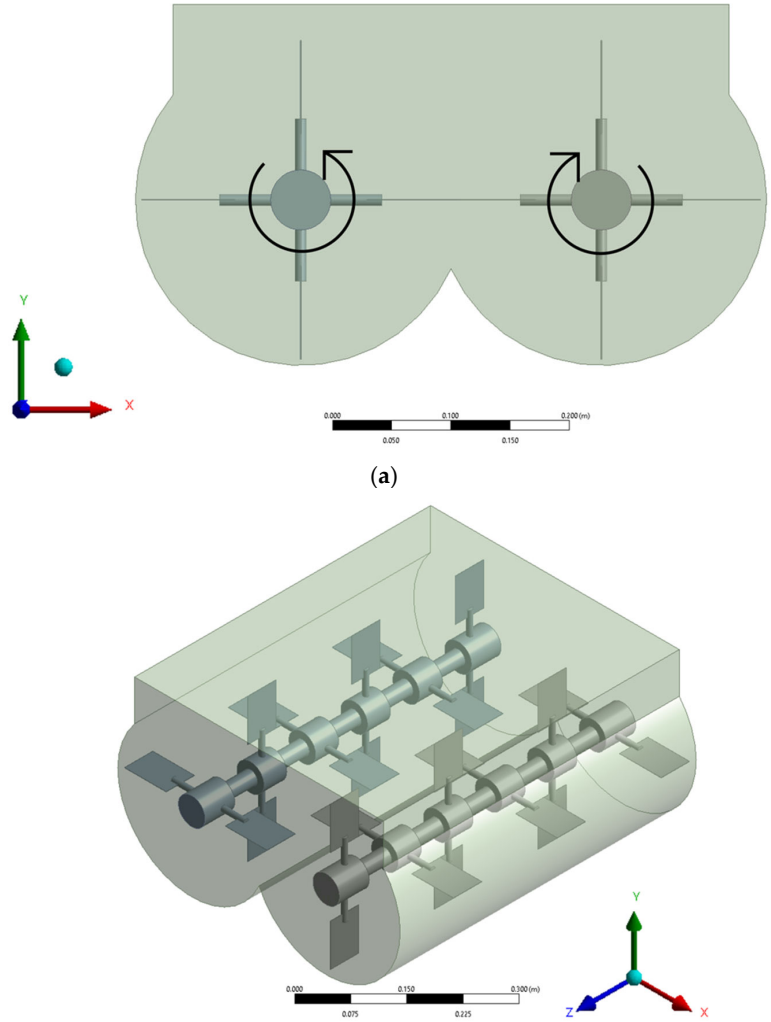

Figure 1. Mixer's geometry used in the base case simulation; (**a**) Front view, and (**b**) Isometric view.

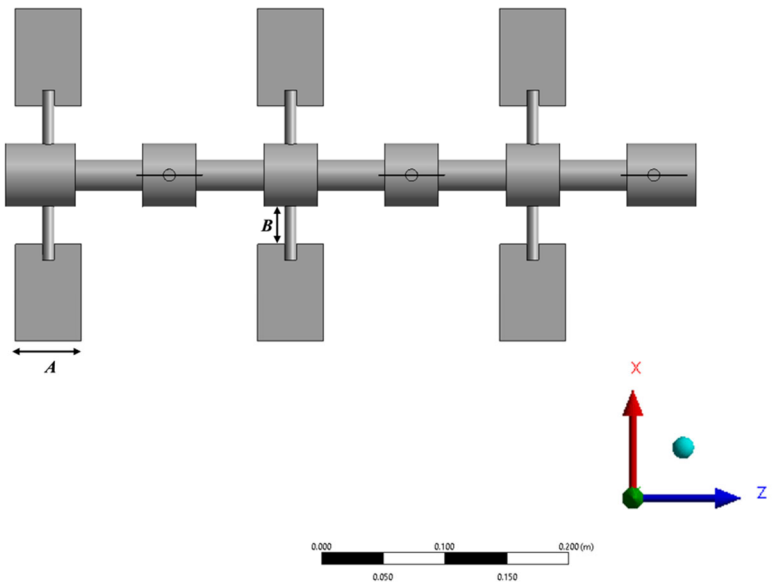

Figure 2. Impeller's geometry used in the base case simulation.

2.2.2. Mixer's Design Parameters

In this section, all the investigated mixer configurations are mentioned in detail. Three different mixer configurations' parameters are studied, including gap (distance between the blades and mixer's wall), width, and angle of blades. The length of the impellers (B in Figure 2) is altered to adjust the gap between the blades and the mixer's wall. Six blade gaps are investigated: 0.25 d_p, 0.5 d_p, 0.75 d_p, 1 d_p, 1.5 d_p, and 2 d_p where d_p stands for particle diameter, which is 5 mm in the simulations. Moreover, the effect of paddle width (A in Figure 2) on the mixing quality is investigated. Like the investigated mixer in our previous study [3], the paddle width is selected to be 0.053 m for the base case in the current study. Different multiplications of the base paddle width are selected to examine the impact of the paddle width on the particle mixing process, including 0.25, 0.5, 0.75, 1.0, and 1.25 times the base paddle width (A). Moreover, to examine the influence of the paddle angle on the mixing quality, the mixing process is simulated using various paddle angles. In this study, the angle between the blade surface and the horizontal z-direction is referred as the paddle angle (α). Four different paddle angles are selected: 0°, 30°, 45° and 60°. Figure 3 displays a schematic of the impeller blade's angle configurations used in our simulations (0°, 30°,45°, and 60°).

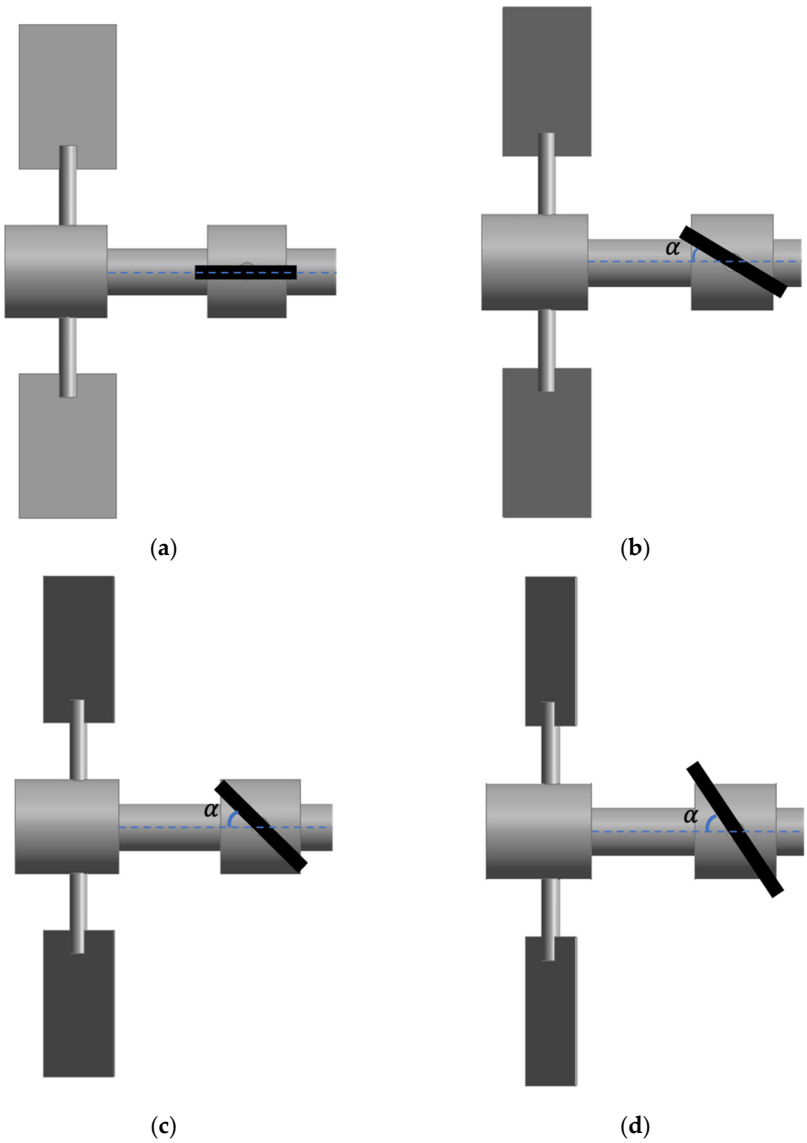

Figure 3. Schematic of various configurations for paddle angle (**a**) α = 0°, (**b**) α = 30°, (**c**) α = 45° and (**d**) α = 60°.

2.2.3. Particles' Properties

Spherical glass beads with a density of 2500 $\frac{kg}{m^3}$ and a diameter of 5 mm are employed in this study. A total of 40% of the mixer's volume is loaded with particles (in total 264,600 particles). First, 132,300 blue particles with a diameter of 5 mm are added to the mixing system. The particles are allowed to settle under the gravitational force, and when the average particle kinetic energy (K_e) of all particles is less than 1.0×10^{-7} J, then 132,300 red particles with the same diameter are added on top of the blue particles and allowed to settle under the gravity force. In this study, this loading configuration is known as the top-bottom loading arrangement. In order to analyze the mixing process, the particles are colored red and blue, but their material properties are the same. The impellers remain stationary as the particles are loaded into the mixer during the simulation. When the particle loading step is performed, and the average kinetic energy of all particles is less than 1.0×10^{-7} J, the impellers are allowed to rotate at 40 RPM for 30 s of simulation time. Figure 4 illustrates the initial state of the mixing system after the generation of all the particles from various views.

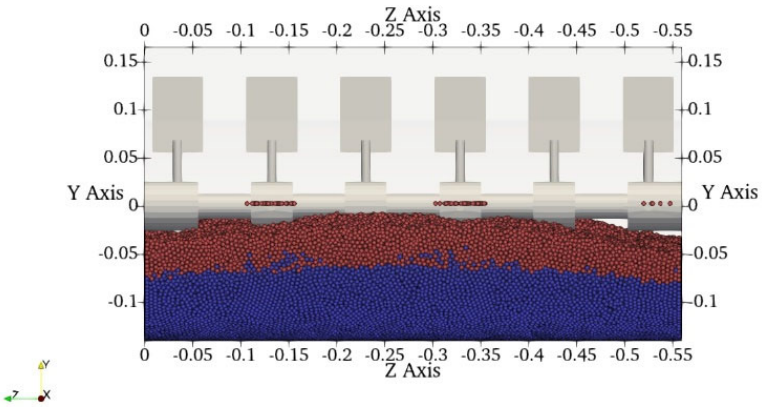

(**a**)

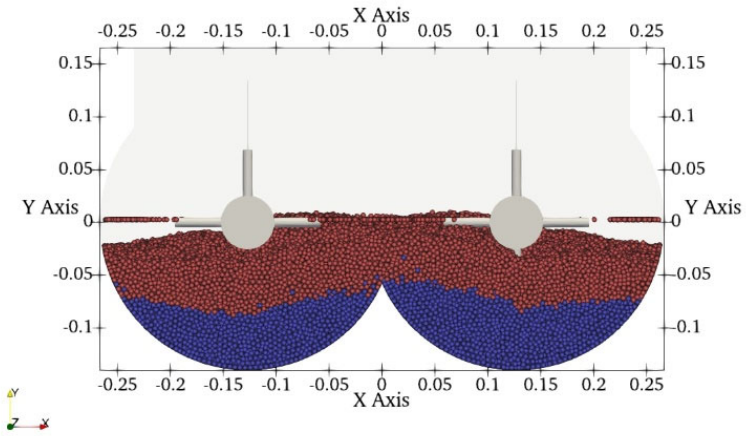

(**b**)

Figure 4. The initial state of the mixing system after loading all the particles; (**a**) Side view, (**b**) Front view.

2.3. Mixing Characterization Analysis

2.3.1. Mixing Performance

The relative standard deviation (*RSD*) mixing index is employed to quantify the performance of the mixing system under examination [2,9,29–33]:

$$RSD = \frac{\sigma}{C_{avg}} \tag{1}$$

where C_{avg} denotes the average concentration of all the samples and σ stands for standard deviation, which is calculated as follows:

$$\sigma = \sqrt{\frac{1}{N-1}\sum_{i=1}^{N}(x_i - x_m)^2} \tag{2}$$

where x_i, x_m, and N are the number fraction of each type of particle presented in grid i, the average number fraction of particles presented in all grids, and the total number of grids, respectively.

2.3.2. Solid Dispersion

In our previous study [3], it was found that the dominant mixing mechanism in the mixing system is diffusion. Thus, the diffusion intensity as another microscopic property of the system is calculated, which helps to characterize the mixing system under investigation. The diffusion intensity of the particulate flow is quantified by calculating the diffusion coefficient. Several studies have shown that mixer's geometrical structure greatly influences diffusion coefficients [2,34]. The diffusion coefficient is defined as [3]:

$$D_{ij} = \frac{\left\langle \left(\Delta x_i - \overline{\Delta x_i}\right)\left(\Delta x_j - \overline{\Delta x_j}\right)\right\rangle}{2\Delta t} \tag{3}$$

where D_{ij} denotes the diffusion coefficient in direction i due to a concentration gradient in the direction j. Δx_i and $\overline{\Delta x_i}$ represent the particle displacement and mean displacement during the time interval (Δt), respectively. Angle bracket $\langle\ \rangle$ denotes the averaging over all the particles for the contents within those brackets.

2.3.3. Granular Temperature

The degree of random movement of particles is measured by the granular temperature [22]. In addition, it can be used to evaluate how particles diffuse and segregate. The diffusive mechanism plays a crucial role in particle mixing in systems with higher granular temperatures [35]. The granular temperature is defined as follows [36]:

$$T = \frac{1}{di}\langle u'u'\rangle \tag{4}$$

where u' and di denote each particle's velocity fluctuation at a given time in a control volume and the spatial dimension, sequentially. Moreover, $\langle\ \rangle$ averages within the control volume. This study uses the same control volume and time interval as our previous study ($\Delta t = 0.1$ revolution time and control volume size = 4 d_p) [3].

Temperature profiles at granular scales can also assist with the development of continuous models to describe the mixing system [37]. In this study, granular temperature values are calculated on a plane along the shaft (contour plot) as well as in series of control volumes (highlighted in blue in Figure 5) and are reported in the results section to examine the effect of impeller design on the granular temperature distribution in the mixer. The plane is selected in the location where it is fully submerged in the particle mixture during the mixing process, and the control volumes are selected at the tip of the impeller's

blades. Figure 5 illustrates the plane and the control volumes used in the calculation of the granular temperature.

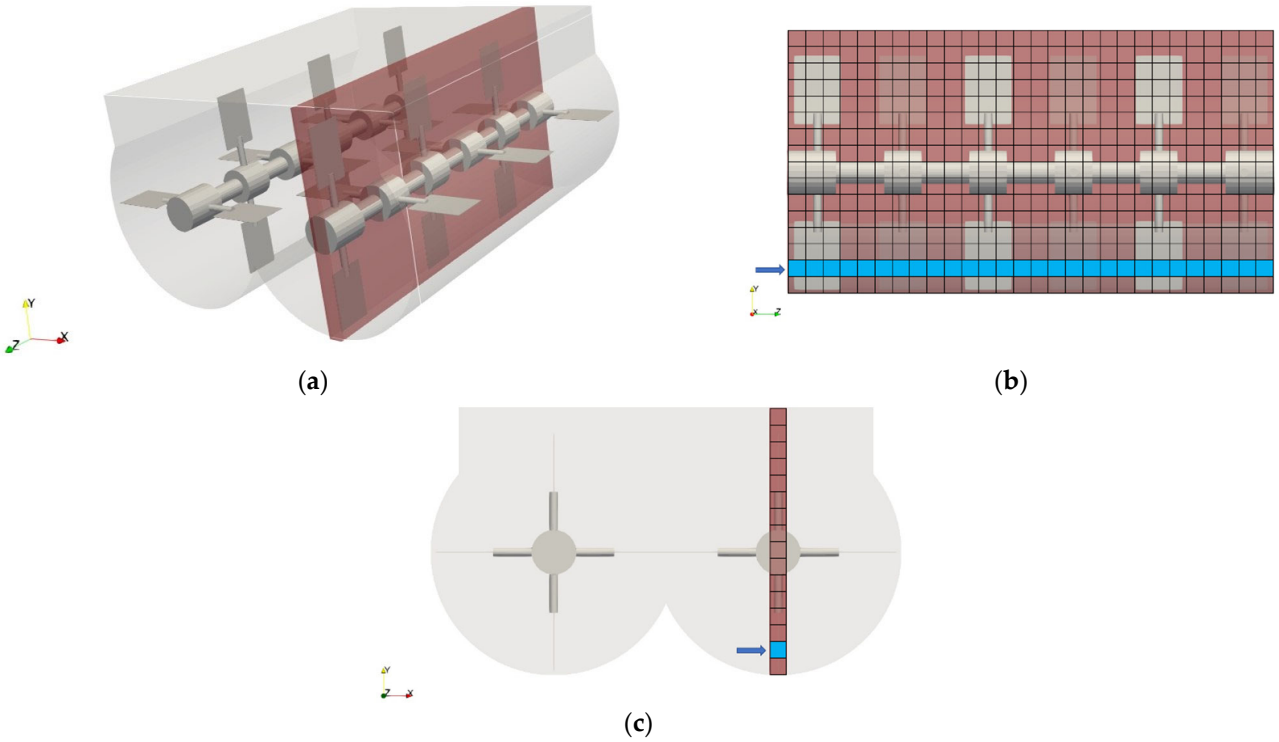

Figure 5. Plane and control volumes used for calculation of granular temperature profile from (**a**) Isometric, (**b**) Side, and (**c**) Front view.

2.3.4. Force Acting on Particles and Power Consumption

As mentioned in Section 2.1, contact and gravitational forces are only considered forces acting on particles in each timestep. During the mixing process, both contact and gravitational forces play a vital role in determining the hydrodynamics of the particulate flow [19]. Therefore, in this study, to analyze the granular flow behavior, mean and time-averaged forces acting on particles are calculated. The mean force (F_m) is defined here as the average forces acting on all particles at a specific time. The time-averaged force (F_t) is determined by averaging the mean forces over entirety of the mixing time (30 s). In addition, to show the system's force profile, the time-averaged force acting on all the particles on a plane along shaft (depicted in Figure 5) is calculated and reported in each simulation case for comparison. It is important to also investigate how the power and torque values change when modifying the impeller configuration. In general, power consumption is also a main parameter in evaluating the performance of a mixing system [38,39]. Thus, to evaluate the performance of the mixer, the power consumption (P) for each impeller is calculated as follows:

$$P = \frac{2\pi}{60} \times s \times M \tag{5}$$

where s and M are impeller rotational speed (RPM) and torque acting on the impeller (N.m), respectively. In this study, since the mixer contains two parallel impellers, the system's total power consumption can be calculated from the summation of the power consumption of each impeller.

3. Results and Discussion

In this section, the effects of the paddles' configurations (paddle's angle, width, and gap) on the performance of the mixing system are examined. The mixing performance,

diffusivity coefficient, particles' velocity components, the total force acting on particles, and power consumption of the mixer are compared for various paddle configurations.

3.1. Mixing Performance

The selected control volume's size for RSD calculations significantly affects the RSD values [2–4,6,14]. Thus, in analogy to previous studies [10,24], sensitivity analysis needs to be carried out to identify the control volume's size. To do so, the RSD values are calculated for the base simulation run (40 RPM, 40% fill level, and 0° paddle angle with TB initial loading) for different control volume sizes. Based on the results presented in Figure 6, further reductions in control volume's size smaller than $4 \times d_p$ had a negligible impact on RSD values. Accordingly, to reduce the post-processing computational time, the control volume's size of $4 \times d_p$ (0.02 m) is selected for further RSD calculations in this study. Using the selected control volume's size, the system is divided into 28, 16, and 28 cube bins sequentially in the x, y, and z directions.

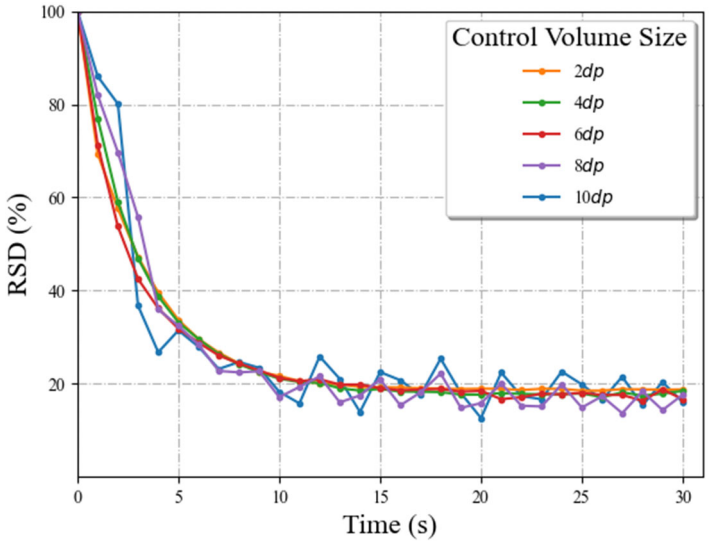

Figure 6. Sensitivity analysis for the effects of control volume size on the RSD values.

Figure 7 demonstrates the influence of paddle angle on the mixing performance. The RSD values derived from the DEM simulation versus time are depicted in Figure 7, which compares the RSD indices for four different paddle angles when the fill level is 40%, the impellers speed is 40 RPM, the paddle gap is 1 d_p and the paddle width is 1 A. After a rapid initial decline, all the mixing indices eventually fluctuate around their fixed value. However, the time that they reach the steady-state condition varies for each case. As seen in Figure 7, for a paddle angle of 30° to 60°, the mixing status is significantly influenced by the paddle angle during mixing. As can be seen in Figure 7, for the top-bottom initial loading pattern with a 40% fill level and 40 RPM impeller speed, the mixer with a 60° paddle angle has the worst mixing rate compared to other cases in all mixing times. However, toward the end of the mixing time (i.e., after 25 s), the RSD values obtained from the mixer with a paddle angle of 60° finally reach the vicinity of RSD values yielded by other paddle angle cases. Moreover, increasing the paddle angle from 0° to 45° deteriorates the mixing performance at the initial stages of mixing (before 6 s when comparing 0° and 30° and before 15 s when comparing 45° with 0° and 30°). However, after 15 s of the mixing process, the mixing performances for 0°, 30°, and 45° paddle angles reach almost the same values. Figure 7 illustrates that the mixing performance (RSD) reduces monotonically with the rake angle in the range of 30–60° when paddle width and gap are held constant. Thus, increasing the paddle angle in the mixer generally lessens the system's mixing performance. However, the previously reported results showed that a better mixing performance was attained for the paddle angles of both 30° and 45° than that for a paddle angle of 0° for

a single paddle blender [2]. This difference can be explained by the fact that the mixing in the twin paddle blender is partly dependent on the movement of particles from one vessel to the other one. Thus, in a twin paddle blender, the number of particles that can be transferred between two vessels was the highest using a 0° paddle.

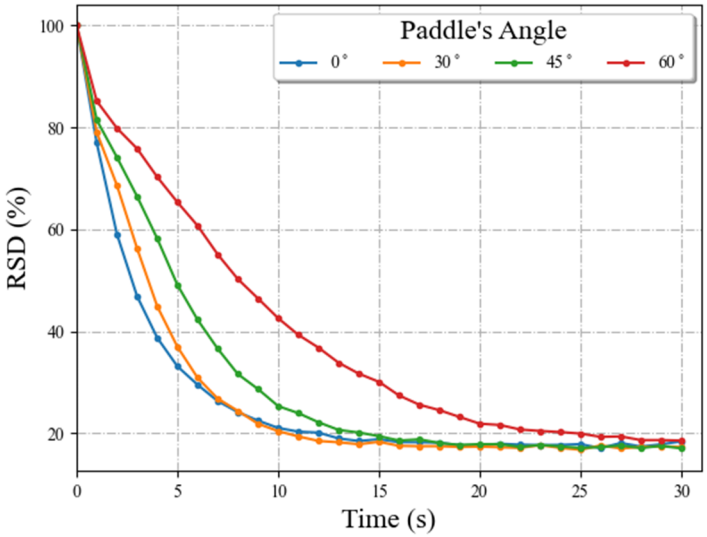

Figure 7. RSD values versus time for various paddle angles.

Figure 8 illustrates the mixing behaviors of four different impeller's blade angles at different time instants when the fill level is 40%; the impeller rotational speed is 40 RPM, the paddle gap is 1 d_p, and the paddle width is 1 A. These figures show how mixing takes place over time. Initially, the red and blue particles are entirely separated. Over time, the particles are gradually mixed. After the simulation is completed, a mixture with a high mixing quality is obtained (t = 30 s). Comparing the particle distribution of four different impellers' configurations reveals some differences. Particles in the mixer with a 0° paddle angle are transported radially in the mixer by impellers (Figure 8a). However, the impellers pushed particles along the z-direction toward the shaft in other cases (Figure 8b–d). Moreover, by comparison of the simulations' snapshots (especially for the initial stages of the mixing process), it can be found that the particle distribution is more homogeneous for the mixer with a paddle angle of 0°. These results also confirm the trends that are reported in Figure 7.

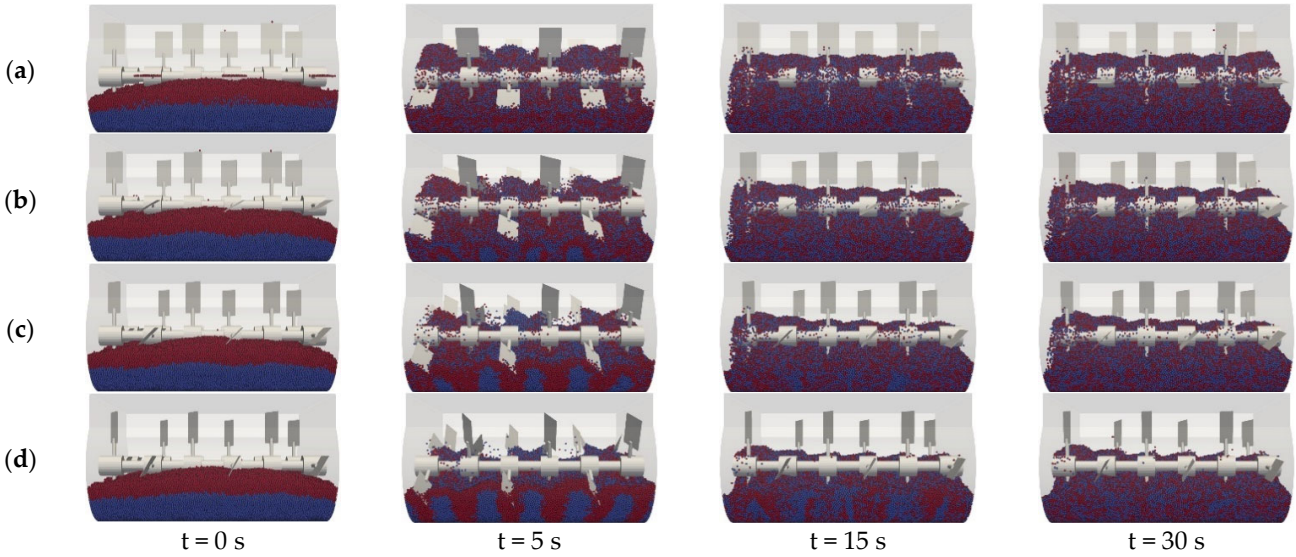

Figure 8. Mixer's snapshot with various paddle angles at different time instants: (**a**) 0°; (**b**) 30°; (**c**) 45°; (**d**) 60°.

Figure 9 illustrates the variation in mixing performance when changing paddle width (RSD mixing index versus time). As can be seen, paddle width has a significant influence on the mixing efficiency. As expected, the mixing performance improved as a wider paddle was employed. However, increasing the paddle width from 1.0 A to 1.25 A did not affect the mixing index significantly. The results in Figure 9 show that the blade width in the paddle mixer is a critical parameter for achieving better mixing. This observation can be explained by the number of particles that can be touched and moved by the impellers using various paddle widths due to the difference in the paddle surface area. When 0.25 A and 0.5 A are used as the paddle width, several particles are not touched by the impellers. Thus, those parts of the particle bed cannot show a homogenous mixture, which results in an inferior mixing performance (low RSD value). Although using the narrow paddle width (0.25 A and 0.5 A) is not popular in industrial applications, in this study, we used these paddle widths to examine the impacts of paddle width on the mixing behavior of the double paddle mixer.

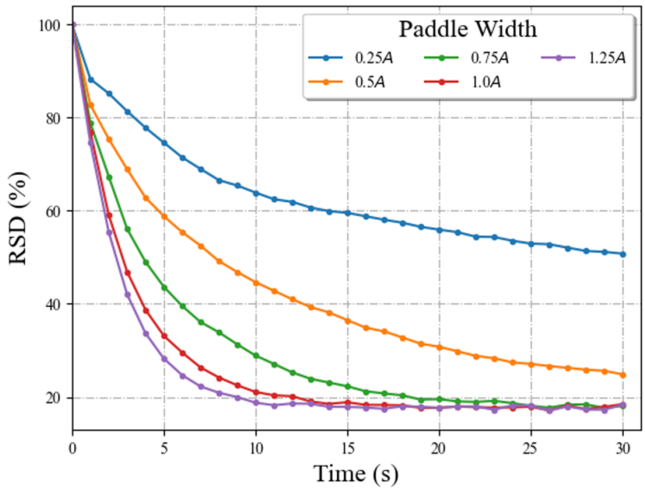

Figure 9. RSD values versus time for various paddle widths for 40 RPM, 40% fill level and 0° paddle angle.

Figure 10 illustrates the RSD values calculated during the mixing process for the mixer with various paddle gaps. Various paddle gaps from 0.25 d_p to 2.0 d_p are considered in the simulations for a paddle angle of 0°. This figure demonstrates a negligible difference in RSD values using various paddle gaps in the system. Thus, it is concluded that the paddle gap has a minor influence on the mixing progress in the double paddle blender.

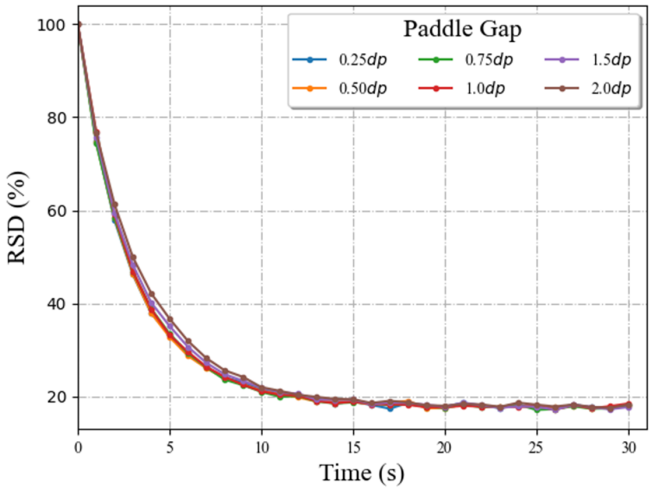

Figure 10. RSD values versus time for various paddle gaps for 40 RPM, 40% fill level and 0° paddle angle.

3.2. Particle Diffusivity

This section of results explores the effect of the paddle angle on diffusion in the mixing system. As observed in our previous study [3], the dominant mixing mechanism in the double paddle blender was diffusion. Thus, the diffusivity coefficient can be employed to compare the mixing performance for various paddle angles. As reported in the literature [2,3], the diffusivity coefficient values significantly depend on the selected time interval (Δt), as indicated in Equation (3). Therefore, in this study, a sensitivity analysis is conducted on the diffusivity coefficient values for various time intervals. After testing different values for Δt, the diffusivity coefficient becomes independent of Δt values, where the time interval is equal to or less than $1/4$ of the impeller's revolution time. Thus, in the post-processing calculation in this study, $1/4$ of the impeller's revolution time is selected for the time interval ($\Delta t = 0.375$ s). Table 1 summarizes the diffusion coefficients for different simulations using various paddle angles.

Table 1. Diffusion coefficient calculated for various paddle angles (for 30 s simulation of 40% fill level and 40 RPM).

	$\alpha = 0^\circ$	$\alpha = 30^\circ$	$\alpha = 45^\circ$	$\alpha = 60^\circ$
$D_{xx}(\mathrm{m^2/s})$	2.13×10^{-3}	1.28×10^{-3}	6.70×10^{-4}	2.60×10^{-4}
$D_{yy}(\mathrm{m^2/s})$	1.82×10^{-3}	1.21×10^{-3}	7.30×10^{-4}	3.56×10^{-4}
$D_{zz}(\mathrm{m^2/s})$	3.88×10^{-4}	6.00×10^{-3}	6.10×10^{-4}	3.80×10^{-4}

As shown in Table 1, the paddle angle of 60° produces the lowest values of diffusion coefficients in all directions. These results can explain the poor mixing performance obtained from 60 compared to all other impeller configurations analyzed in this research. These results also can clarify the trends reported in Figures 7 and 8. Consistent with our previous study [3] and other literature [4], in this study, D_{xx} and D_{yy} are higher than D_{zz} in all the simulation cases presented in Table 1. A higher diffusion coefficient in x and y directions indicates that mixing mainly occurs in these directions. Thus, mixing performance comparison can be performed by comparing the diffusion coefficients in x and y directions. Moreover, Table 1 reveals that diffusivity coefficients decrease in x and y directions as the paddle angles increase. This observation can confirm the RSD values' trends presented in Figure 7, in which when the paddle angles increase, the mixing efficiency decreases.

3.3. Mixing Kinetics: Velocity Distribution and Granular Temperature

Figure 11 illustrates the spatial velocity distribution of the particles. It can be seen that between two adjacent blades, most of the particles are stationary, while those near the impellers achieve relatively greater velocities. Moreover, quantitative comparisons are conducted by calculating the probability density distributions of velocity components in the x, y, and z-axis (depicted in Figure 12). Probability density distributions around zero velocity tend to be normal distributions in all directions, indicating that most particles in the mixer remain stationary. Figure 12 also reveals that more particles in the mixer with paddle angles of 60° and 45° are stationary, followed by the mixer with paddle angles of 30° and 0°. This observation is inconsistent with what is shown in Figure 11, where increases in the paddle angle increase the number of stationary particles.

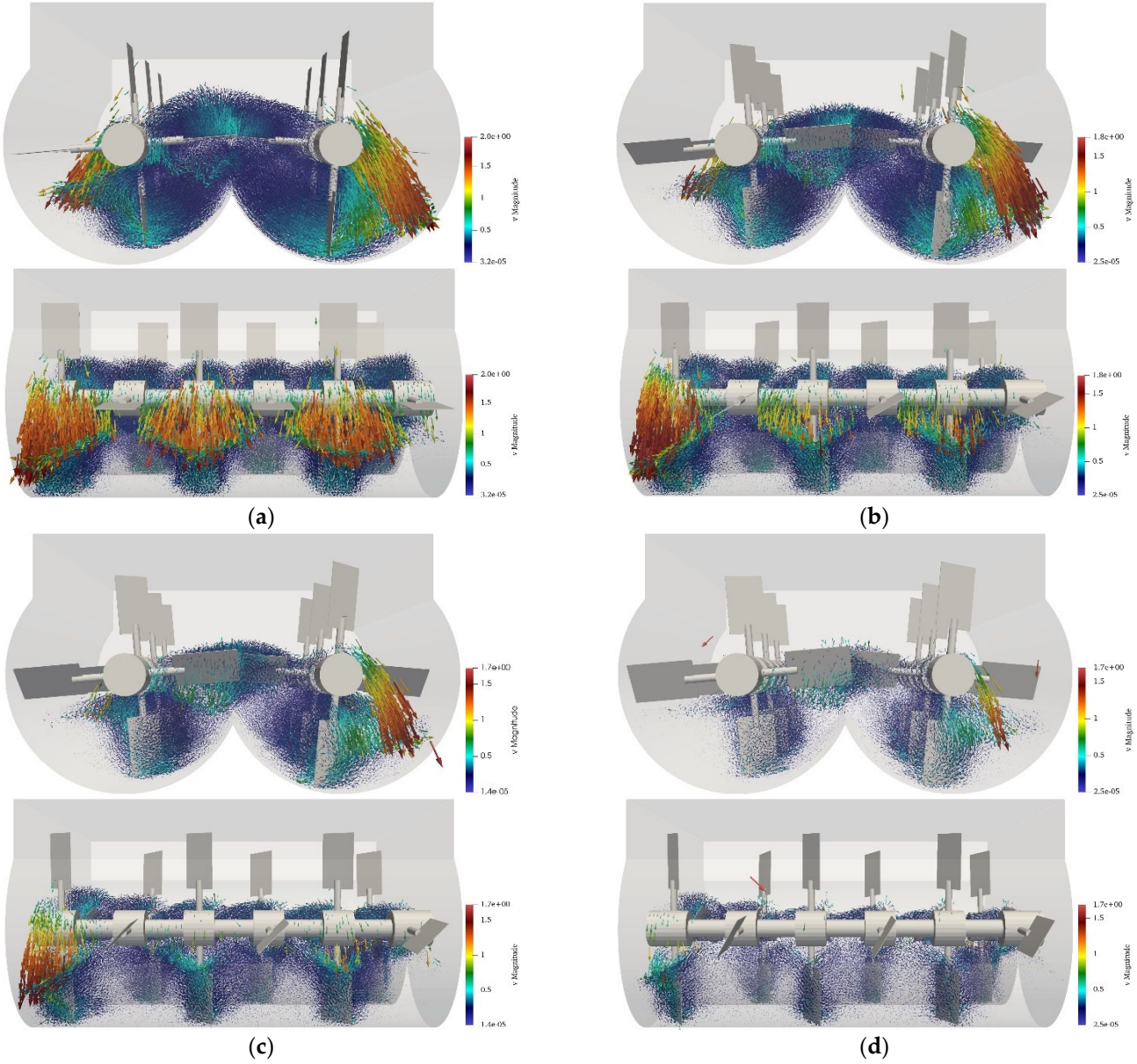

Figure 11. Spatial particles' velocity distribution at t = 30 s: (**a**) 0°; (**b**) 30°; (**c**) 45°; (**d**) 60°.

By examining Figure 12a–d, it can be deduced that the velocity *y*-component for all the cases shows a right-skewed distribution, representing the direction of vertical movement of particles in all the cases. However, by increasing the paddle angle from 0° to 60°, the skew in the graphs decreases. Thus, the particles' movement in the *y*-direction decreases by increasing the paddle angle. Moreover, increasing the paddle angle enhances the left-skewed distribution in the *z*-axis, which indicates that the particles move more in the opposite of the *z*-direction (along the shaft). The probability distributions of the velocity *x*-component for the four cases are rather symmetric and near to normal distributions, showing that the probability of particle motion in the *x*-direction is quite the same for all cases.

Figure 13 illustrates the time-averaged granular temperature along the *z*-direction for various paddle angles. This figure shows that increasing the paddle angle decreases the granular temperature values, which suggests lower particle velocity fluctuations and more uniform particle flows at high paddle angles. As reported by Boonkanokwong et al. [22], higher granular temperature values in a mixing system indicate higher diffusive mixing (particle diffusivity). Thus, the results in Figure 13 imply that a lower paddle angle in

the mixing system provides a higher diffusive mixing of particles. These findings are consistent with the results presented in Section 3.2. These results can also explain the findings in Section 3.1, where a lower paddle angle intensified the particles' chaotic motion, consequently improving mixing efficiency (lower RSD values). Figure 13 also demonstrates that for all the paddle angles, there are five minimum granular temperature regions and six sections with high granular temperatures. The minimum granular temperatures occur in the regions between the paddle blades, and the sections with high granular temperatures represent the areas swept by six paddle blades. Ebrahimi et al. [2] and Golshan et al. [40] also reported greater granular temperatures near the impeller when studying a single paddle blender and a Nauta batch blender, respectively.

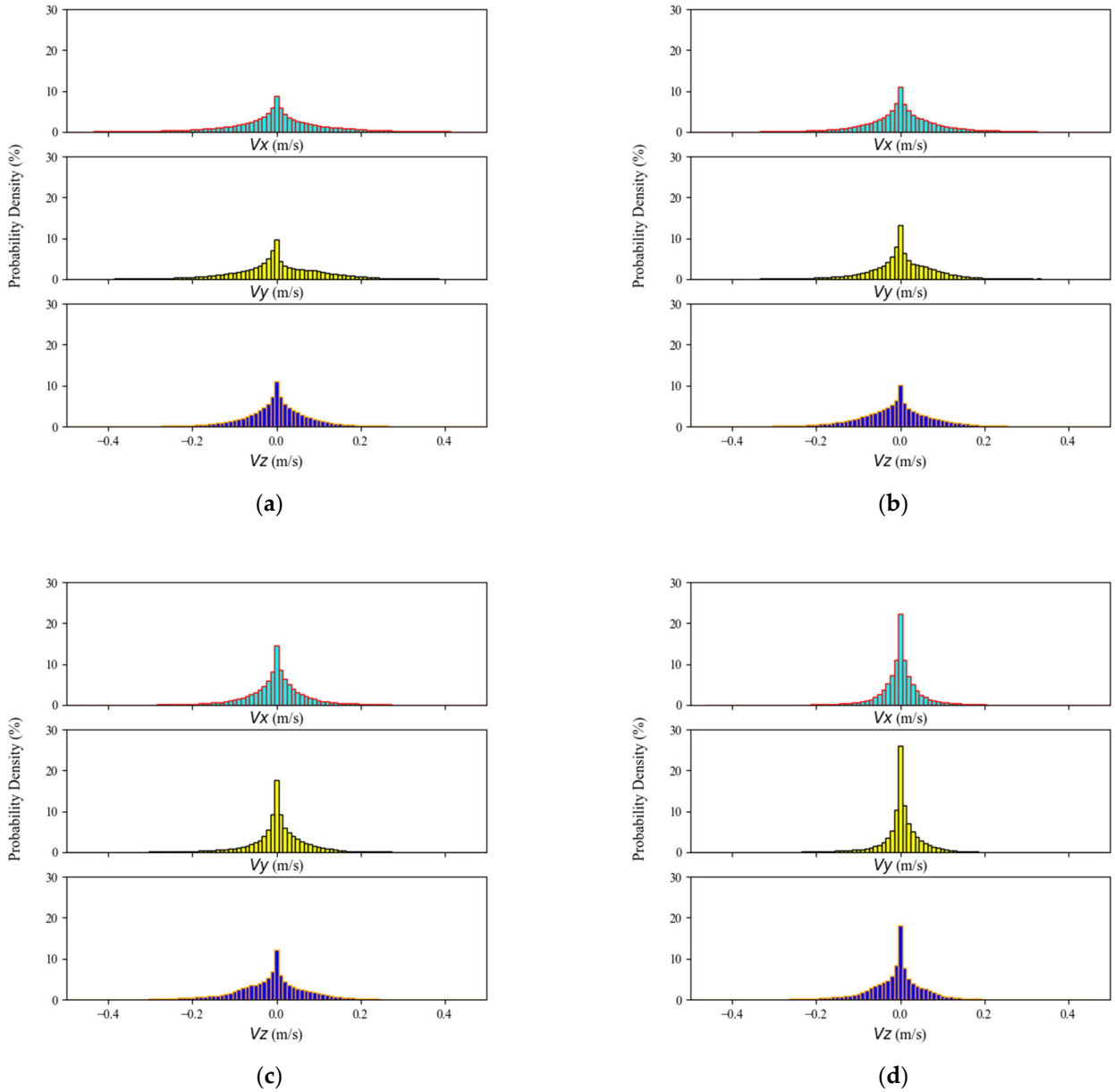

Figure 12. The probability density distributions of the *x*, *y*, and *z*-axis velocity components at t = 30 s for paddle angle of (**a**) 0°, (**b**) 30°, (**c**) 45° and (**d**) 60°.

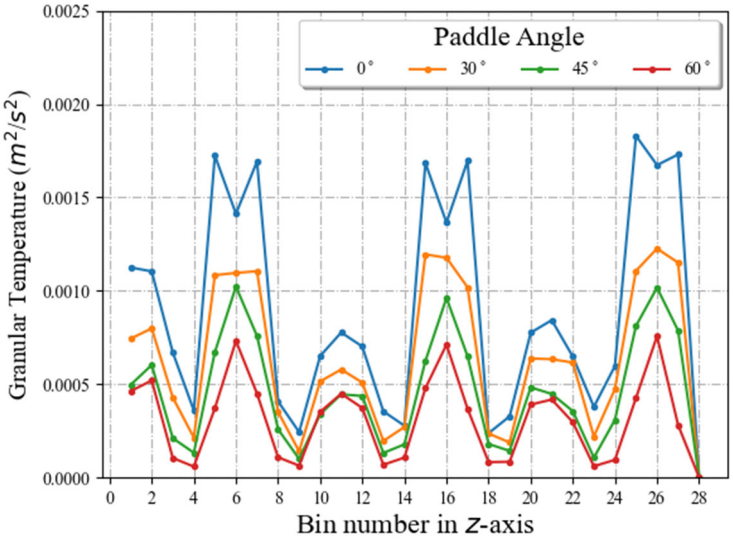

Figure 13. Granular temperature in a line along z direction for various paddle angle of 0°, 30°, 45° and 60°.

3.4. Forces Acting on Particles and the Mixer Power Consumption

This section covers the influence of the paddle angle on the magnitude of the forces (exerted by the impellers, vessel, and particles) acting on particles and the mixer power consumption. Figure 14 compares forces acting on the particles in the system for the mixer with different paddle angles. This figure shows that the mean force acting on particles imparted by the 0° paddle angle impeller is the largest compared to the mean forces acting on particles in all other angles. Moreover, it is found that a higher paddle angle results in lower mean forces acting on particles. This result is in good agreement with what was observed by Siraj et al. [16] and Chandratilleke et al. [21]. According to their findings, both tangential and normal forces acting on particles reduce with increasing the paddle angle. This observation can be explained by the number and intensity of the contact points (both particle–particle and particle–geometry) in the system. Using the higher paddle angles causes particles to slide over the surface of the paddles. Therefore, the number of particles lifted by a paddle with a lower angle is higher than the number of particles lifted by a paddle with a higher angle. Moreover, the paddles with a lower angle can elevate particles into higher positions (y-direction). Consequently, larger forces are created when large numbers of highly raised particles are dropped from the paddle surface at a low angle onto the particle bed compared to those when high-angled paddles are employed.

Therefore, compared to a paddle angle of 0°, when the 30°, 45°, or 60° paddle angles are used, the number of particles lifted is much lower, and particles raised from the mixture drop quickly onto the surface of the particle bed. As a result, less force is applied to the particles in these configurations than at a paddle angle of 0°. Almost no or very few particles are raised from the particle bed when the mixer paddle angle of 60° is used, which explains the minimum force obtained for this configuration. This section quantifies the forces acting on particles as a function of the paddle angle for the double paddle blender. Thus, this is an important conclusion for a mixing system containing brittle materials such as fragile crystals to maintain the integrity of particles by using high paddle angles.

It should be noticed that, in the literature [2,16,21], the mean force reported was spatially averaged over all the contacts in the mixture. Using the results reported in the literature, it may not be possible to identify the regions with the highest forces acting on particles. Thus, in this study, a more refined analysis is reported in order to evaluate the profile of forces acting on particles. Figures 15 and 16 illustrate the forces acting on particles over the line and plane depicted in Figure 5. Figure 15 shows a variation of the time-averaged forces acting on particles in different bins in the z-direction for various paddle angles. As seen in this figure, it can be concluded that increasing the paddle angle decreases

the time-averaged forces acting on particles (as reported in Figure 14). Furthermore, the fluctuations can be attributed to the movement of paddles in the particle bed. Figure 16 illustrates the contour of time-averaged forces acting on particles for various paddle angles. Near the blade tip, particles have maximum forces in all of these contours. There is a minimum force in the center of the impeller shaft, while the maximum force is around 0.08–0.16 N at the tip of the blades.

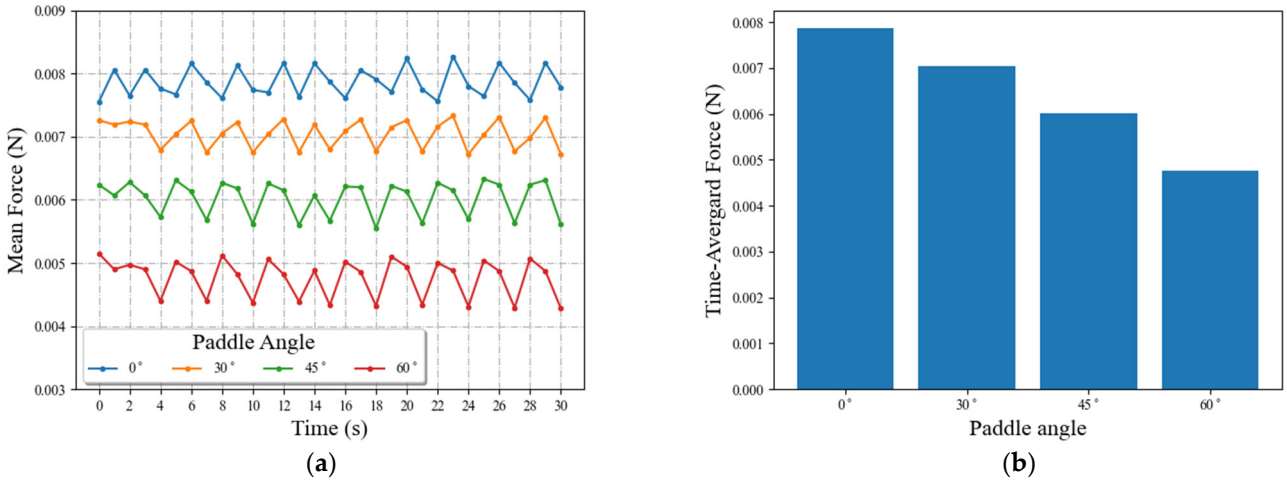

Figure 14. Force acting on the particles in various paddle angles; (**a**) mean force, and (**b**) time-averaged force.

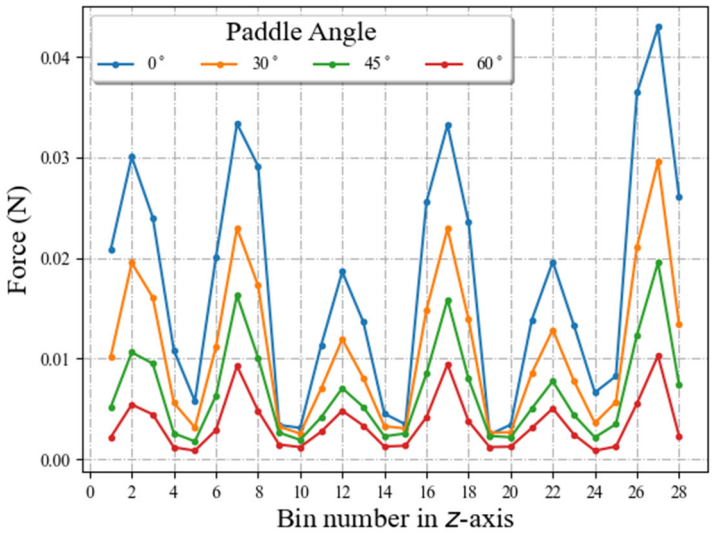

Figure 15. Time-averaged forces acting on particles in a line along *z*-direction for various paddle angle of 0°, 30°, 45°, and 60°.

The effects of paddle angle are also examined on the system's power consumption. Figure 17 depicts the power consumption of the mixer for various paddle angles. Due to the impellers' rotation, and changes in the torque acting on impellers, the power consumption in the system fluctuated during the mixing process. Thus, the mean power consumption is calculated to compare the power consumption for different paddle angles. As shown in Figure 17a, the power consumption for the mixer with a paddle angle of 0–45° is relatively the same. However, the lowest power consumption is achieved for the mixer equipped with a paddle angle of 60°. It is important to note that the mean force described in the paper pertains to the force exerted on particles resulting from particle–particle and particle–wall interactions and is not to be confused with the mean force acting on the impellers. The latter has a direct impact on the torque and power consumption of the mixer. Therefore, it

is crucial to differentiate between the two forces in order to accurately analyze and interpret the findings presented in the paper.

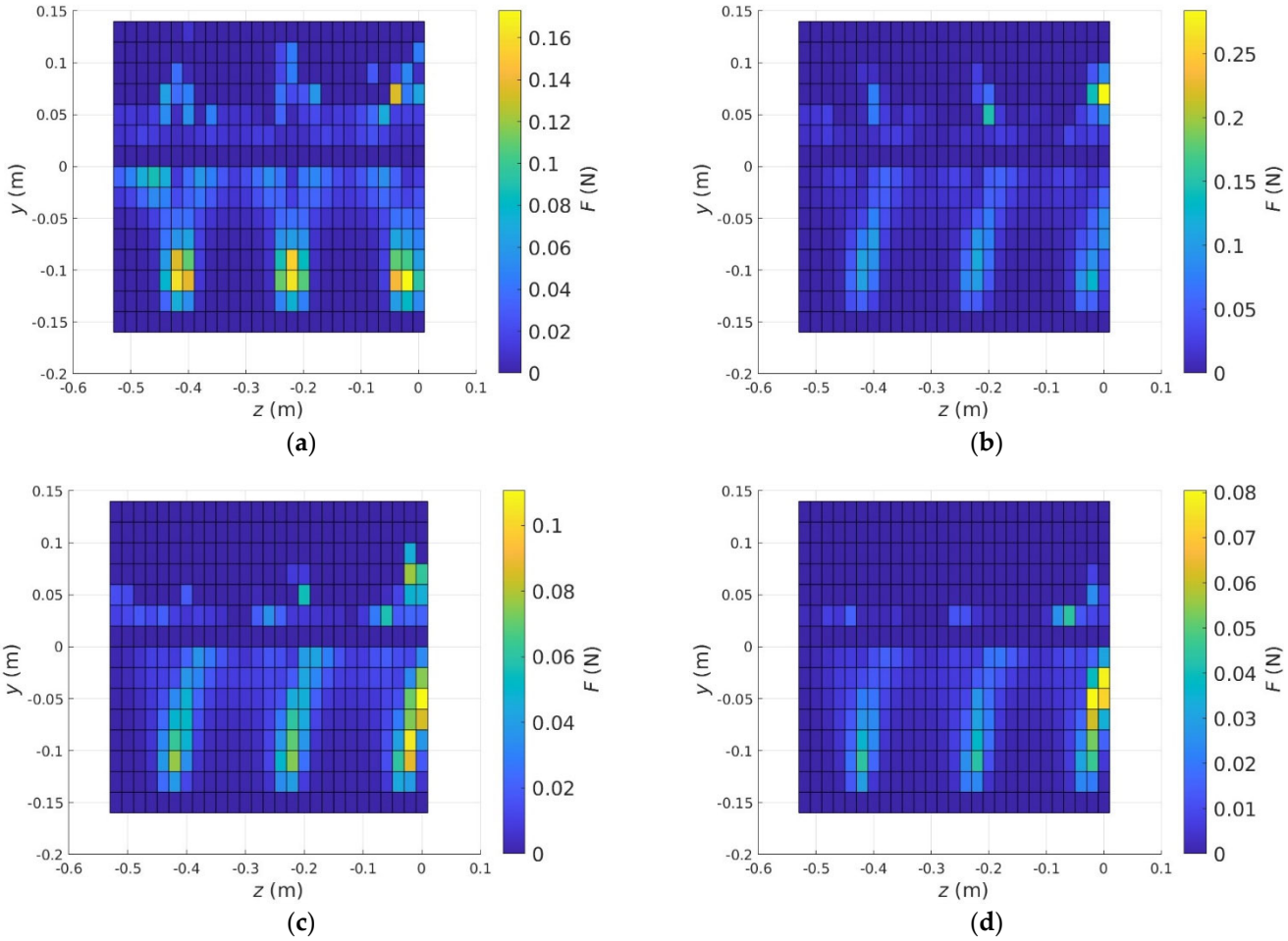

Figure 16. Contour of time-averaged forces acting on particles for various paddle angle of (**a**) 0°, (**b**) 30°, (**c**) 45°, and (**d**) 60°.

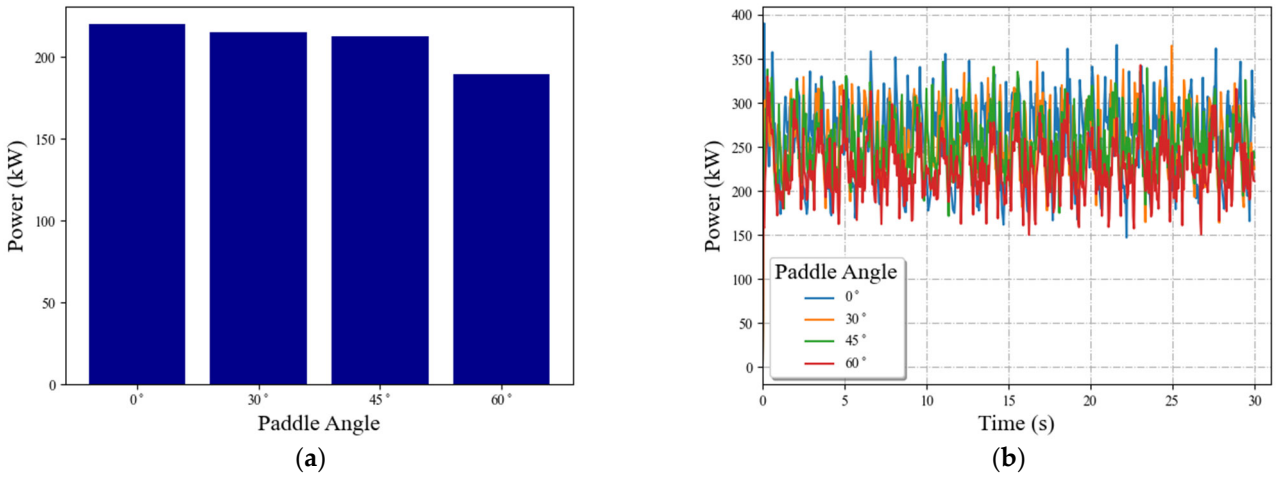

Figure 17. Power consumption of the mixer for various paddle angles: (**a**) mean power consumption and (**b**) transient power consumption.

To examine the effect of the paddle width on powder mixing, forces acting on particles are compared by changing the paddle width (0.25, 0.5, 0.75, 1.0, and 1.25 *A*). Figures 18 and 19 demonstrate that increasing the paddle width increases the time-averaged force acting on the particles. It also can be concluded that the existing bumps in the figure indicate the contact of the impeller's paddle with the particulate flow. The effect of paddle width on the force magnitude acting on particles on a plane along the mixer's shaft can be seen in Figure 20. Thus, by increasing the paddle width, the difference in force magnitude increases in the depicted profile, representing that the forces acting on particles are increased. Based on the results reported in the previous section, the highest mixing rate is achieved using paddles with a large width. However, the forces acting on the particles are increased by using the large paddle width. As mentioned earlier, in industrial applications containing brittle materials, it is necessary to maintain the integrity of the particles by optimizing the forces acting on particles. Consequently, although the blade width of 1.25 *A* obtains the fastest mixing rate, it may not be appropriate for mixing brittle materials.

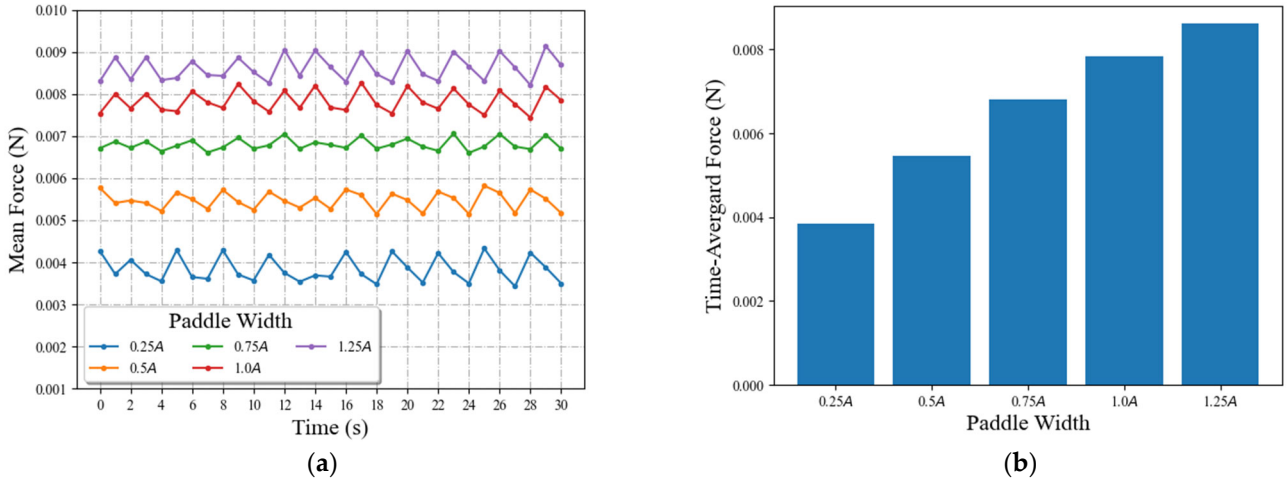

Figure 18. Force acting on particle in various paddle widths: (**a**) mean force and (**b**) time-averaged force.

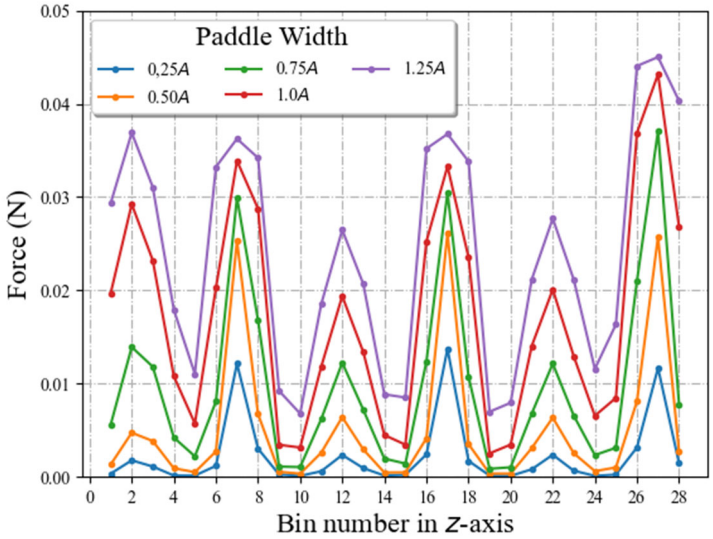

Figure 19. Time-averaged forces acting on particles in a line along *z*-direction for various paddle widths.

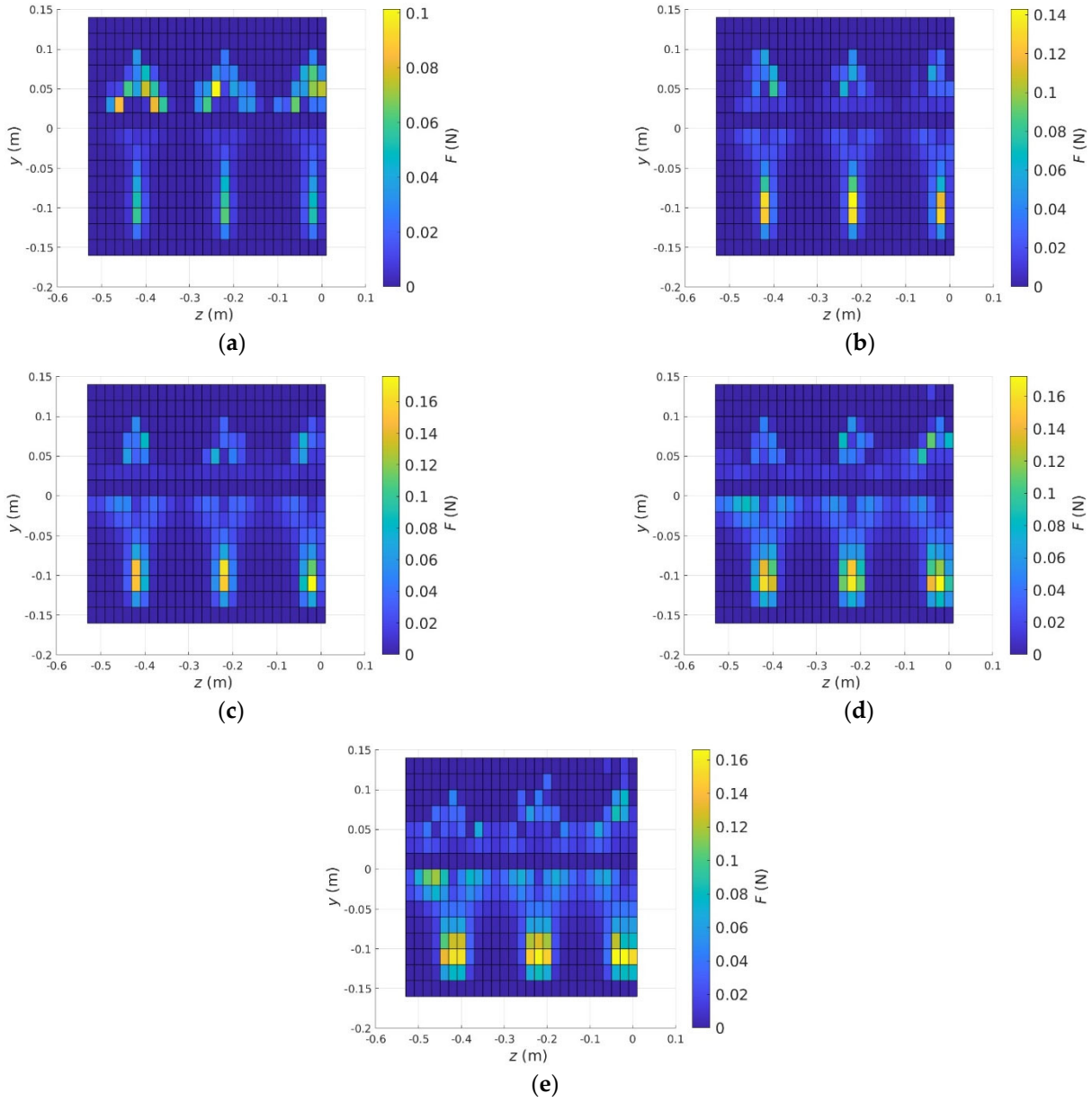

Figure 20. Contour of time-averaged forces acting on particles for various paddle width of (**a**) 0.25 A, (**b**) 0.5 A, (**c**) 0.75 A, (**d**) 1.0 A, and (**e**) 1.25 A.

Figure 21a,b illustrate the impacts of the impeller's paddle width on the mean and transient power consumption of the mixer, respectively. These figures demonstrate that increasing the paddle width led to the enhancement of the system's power consumption. The paddle with 1.25 A has the highest power consumption. Since the mixing rate for the paddle width = 0.75 A is similar to those of higher paddle width (as shown in Figure 9), it can be concluded that the optimum paddle width considering both mixing time and power consumption, should be the paddle blender with a 0.75 A (0.0398 m).

Figure 22 shows the time-averaged forces acting on particles for different impeller paddle gaps. The time-averaged forces acting on particles differ slightly with changing the paddle gap. However, the results indicate that the mixer with a paddle gap of 2.0 d_p imposes slightly less force on particles compared to other paddle gap cases. Furthermore, it can be seen that forces acting on particles reach a maximum value in the mixer with a paddle gap of 0.75 d_p. Following the results presented in Figure 22, the mean power consumption of the mixing system with a paddle gap of 2.0 d_p has a minimum value and a

paddle gap of 0.75 d_p resulted in the highest system power consumption value, followed by 0.5 d_p and 0.25 d_p as shown in Figure 23.

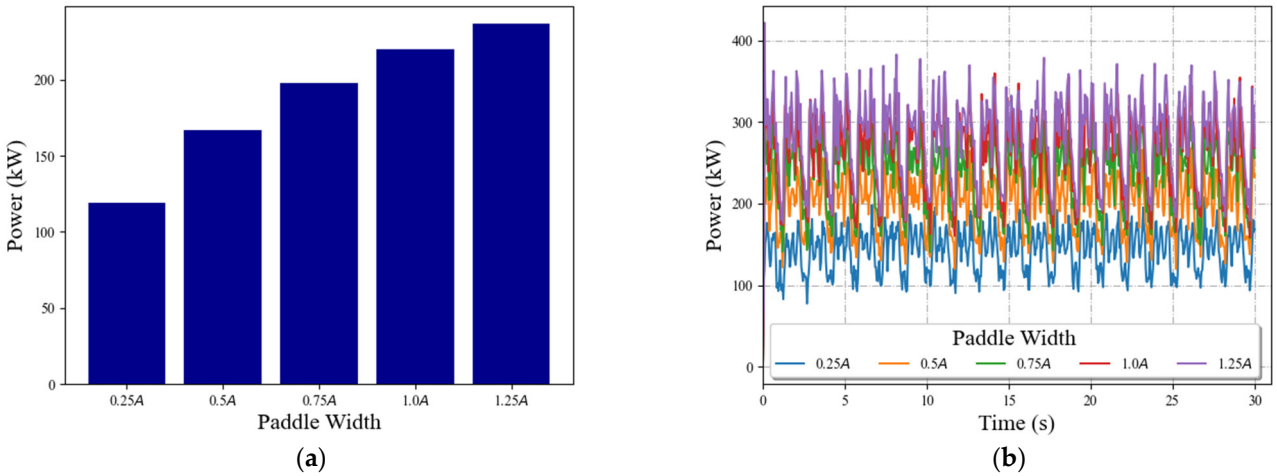

Figure 21. Power consumption of the mixer in various paddle widths: (**a**) mean power consumption and (**b**) transient power consumption.

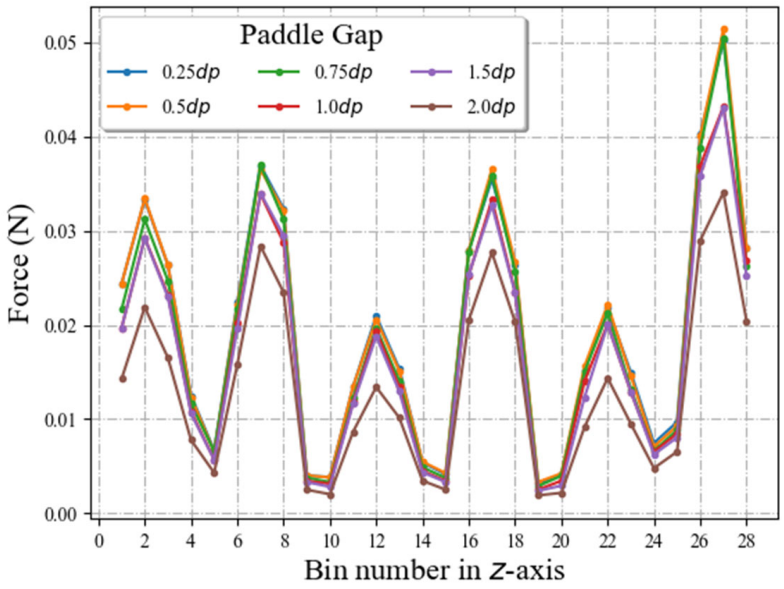

Figure 22. Time-averaged forces acting on particles in a line along z-direction for various paddle gaps.

As shown in Figures 22 and 23, changing the paddle gap slightly changes the mean force acting on particles and the mixer power consumption. This can be explained by the fact that some of the particles are trapped between the tip of the paddle and the mixer's wall during the rotation of the impellers when using paddle gaps smaller than 1.0 d_p. As mentioned earlier in Section 3.1, mixing performance is not affected by changing the paddle gap. Thus, the optimum selection for the paddle gap would be the one that provides the minimum power consumption (2.0 d_p).

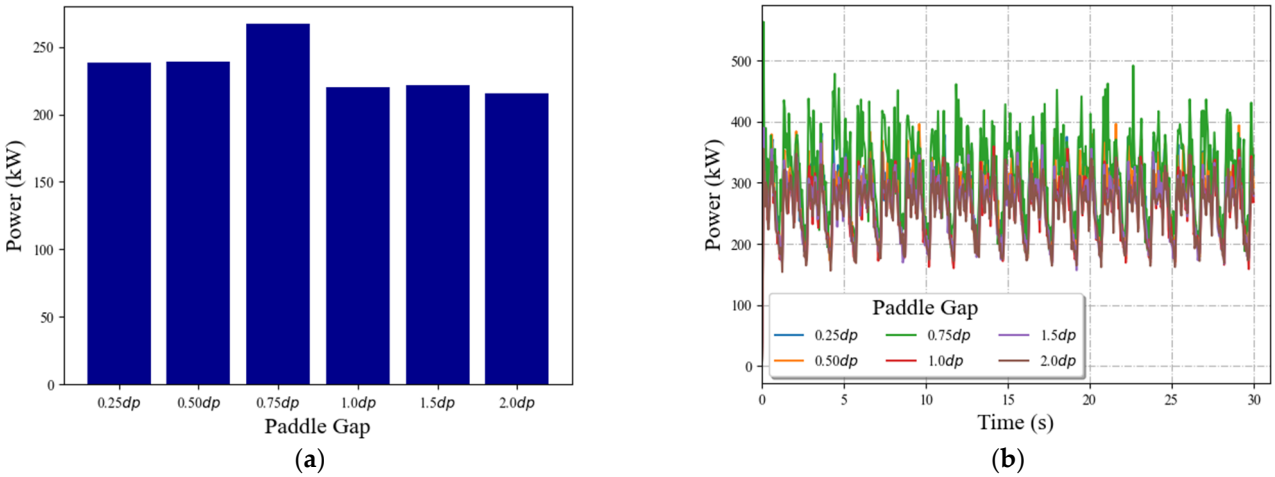

Figure 23. Power consumption of the mixer with various paddle gaps: (**a**) mean power consumption and (**b**) transient power consumption.

4. Conclusions

In this paper, the DEM simulations were performed to examine the particle blending in a twin paddle blender containing cohesion-less, mono-disperse spherical particles. The developed DEM model in our previous research [3] was employed to investigate the influences of the impeller configurations (paddle's angle, gap, and width) on the performance of the mixer. In order to characterize the mixer's performance, RSD values were calculated in each case.

Simulation results indicated that the performance was affected by the paddle's angle and the paddle's width. However, the latter had a more significant effect on the performance of the mixer than the former one. The RSD values of different configurations obtained from simulations revealed that increasing the paddle's angle and decreasing the paddle's width resulted in declining in mixing performance (greater RSD). Generally, the best and second-best mixing performances were achieved for the paddle angle of 30° and 0°, respectively. This was due to the fact that 30° and 0° paddle angles provided the largest and second-largest D_{xx} and D_{yy}. On the other hand, the paddle's gap had a minor influence on the mixing performance in the twin paddle blender.

The analysis of the particles' spatial velocity distribution and probability density distributions of velocity components in the x, y, and z-axis disclosed that the paddle's angle mainly influenced the velocity distributions in the y and z axis. An increase in the paddle's angle increased the number of stationary particles in the system. Analysis of the forces acting on particles and the system power consumption revealed that in comparison with a paddle angle of 0°, when the paddle angles of 30°, 45°, and 60° were used, the number of lifted particles by the impellers was much lower, and these particles dropped quickly on the particle bed surface. Consequently, the angled paddles exerted smaller forces on particles than the paddle angle of 0°. Increasing the paddle width increased the time-averaged force acting on the particles. In addition, due to the enhancement of the paddle's surface area, the system's power consumption was enhanced by increasing the paddle width. The forces acting on particles and the system power consumption varied slightly with changing the paddle's gap.

Finally, it can be concluded that the mixing behavior of the double paddle blender was significantly influenced by the impeller geometry and can be optimized by changing the design parameters of the mixer. Moreover, it was indicated that the DEM approach could be employed as a useful tool to efficiently design powder blenders. However, to expand the knowledge of particle mixing in a powder blender, the effect of particle shape and material on the mixing behavior in such a blender also needs to be investigated.

Author Contributions: B.J.: Conceptualization, Methodology, Software, Validation, Writing—original draft. M.E.: Conceptualization, Methodology, Software, Writing—review and editing, Supervision. F.E.-M.: Conceptualization, Resources, Methodology, Writing—review and editing, Supervision, Project administration, Funding acquisition. A.L.: Conceptualization, Resources, Methodology, Writing—review and editing, Supervision, Project administration, Funding acquisition. All authors have read and agreed to the published version of the manuscript.

Funding: This research was funded by Natural Sciences and Engineering Research Council of Canada (NSERC: RGPIN-2019-04644 and RGPIN-2019-05644).

Institutional Review Board Statement: Not applicable.

Data Availability Statement: Data sharing is not applicable to this article.

Acknowledgments: The financial support of the Natural Sciences and Engineering Research Council of Canada (NSERC: RGPIN-2019-04644 and RGPIN-2019-05644) is gratefully acknowledged.

Conflicts of Interest: The authors report no declarations of interest.

Nomenclature

A	Paddle width [m]	***Greek symbols***	
di	Spatial dimension [-]	α	Paddle angle [°]
d_p	Particle diameter [m]	μ_r	Coefficient of rolling friction [-]
D	Diffusivity coefficient [m^2/s]	μ_s	Coefficient of static friction [-]
e	Coefficient of restitution [-]	ν	Poisson's ratio [-]
F	Force [N]	σ	Standard deviation [-]
G	Shear modulus [Pa]	ω	Particle angular velocity [rad/s]
I	Particle moment of inertia [kg.m^2]	ρ_p	Particle density (kg/m^3)
M	Torque [N.m]	***Subscripts and superscripts***	
m	Mass [kg]	j	Particle j or direction j
P	Mixer's power consumption	i	Particle i or direction i
N	Number of particles	n	Normal direction
v	Particle linear velocity [m/s]	m	average
Δt	Time step [s]	t	Tangential direction or rotational
Δx	Particle displacement [m]	r	Rolling resistance
u'	Fluctuation velocity	g	Gravity
x	Particle's number fraction	c	Contact list

References

1. Paul, E.L.; Atiemo-Obeng, V.A.; Kresta, S.M. *Handbook of Industrial Mixing: Science and Practice*; John Wiley & Sons, Inc.: Hoboken, NJ, USA, 2003. [CrossRef]
2. Ebrahimi, M.; Yaraghi, A.; Ein-Mozaffari, F.; Lohi, A. The effect of impeller configurations on particle mixing in an agitated paddle mixer. *Powder Technol.* **2018**, *332*, 158–170. [CrossRef]
3. Jadidi, B.; Ebrahimi, M.; Ein-Mozaffari, F.; Lohi, A. Mixing performance analysis of non-cohesive particles in a double paddle blender using DEM and experiments. *Powder Technol.* **2022**, *397*, 117122. [CrossRef]
4. Yaraghi, A.; Ebrahimi, M.; Ein-Mozaffari, F.; Lohi, A. Mixing assessment of non-cohesive particles in a paddle mixer through experiments and discrete element method (DEM). *Adv. Powder Technol.* **2018**, *29*, 2693–2706. [CrossRef]
5. Jadidi, B.; Ebrahimi, M.; Ein-Mozaffari, F.; Lohi, A. Investigation of mixing non-spherical particles in a double paddle blender via experiments and GPU-based DEM modeling. *Eng. Proceed.* **2022**, *19*, 12661. [CrossRef]
6. Ebrahimi, M.; Yaraghi, A.; Jadidi, B.; Ein-Mozaffari, F.; Lohi, A. Assessment of bi-disperse solid particles mixing in a horizontal paddle mixer through experiments and DEM. *Powder Technol.* **2020**, *381*, 129–140. [CrossRef]
7. Alchikh-Sulaiman, B.; Alian, M.; Ein-Mozaffari, F.; Lohi, A.; Upreti, S.R. Using the discrete element method to assess the mixing of polydisperse solid particles in a rotary drum. *Particuology* **2016**, *25*, 133–142. [CrossRef]
8. Cundall, P.A.; Strack, O.D.L. A discrete numerical model for granular assemblies. *Géotechnique* **1979**, *29*, 47–65. [CrossRef]
9. Alian, M.; Ein-Mozaffari, F.; Upreti, S.R. Analysis of the mixing of solid particles in a plowshare mixer via discrete element method (DEM). *Powder Technol.* **2015**, *274*, 77–87. [CrossRef]
10. Rodriguez, V.A.; de Carvalho, R.; Tavares, L.M. Insights into advanced ball mill modelling through discrete element simulations. *Miner. Eng.* **2018**, *127*, 48–60. [CrossRef]
11. Halidan, M.; Chandratilleke, G.; Dong, K.; Yu, A. Mixing performance of ribbon mixers: Effects of operational parameters. *Powder Technol.* **2018**, *325*, 92–106. [CrossRef]

12. Wang, S.; Wu, K.; Yu, J.; Zhang, H. Design optimization and scale-up characteristics of a double-helical ribbon reactor for biomass catalytic pyrolysis. *Powder Technol.* **2022**, *399*, 117192. [CrossRef]
13. Jadidi, B.; Ebrahimi, M.; Ein-Mozaffari, F.; Lohi, A. Mixing and segregation assessment of bi-disperse solid particles in a double paddle mixer. *Particuology* **2023**, *74*, 184–199. [CrossRef]
14. Jadidi, B.; Ebrahimi, M.; Ein-Mozaffari, F.; Lohi, A. A comprehensive review of the application of DEM in the investigation of batch solid mixers. *Rev. Chem. Eng.* **2022**. [CrossRef]
15. Chandratilleke, G.; Yu, A.; Bridgwater, J. A DEM study of the mixing of particles induced by a flat blade. *Chem. Eng. Sci.* **2012**, *79*, 54–74. [CrossRef]
16. Siraj, M.S.; Radl, S.; Glasser, B.J.; Khinast, J.G. Effect of blade angle and particle size on powder mixing performance in a rectangular box. *Powder Technol.* **2011**, *211*, 100–113. [CrossRef]
17. Siraj, M.S. Single-blade convective powder mixing: The effect of the blade shape and angle. *Powder Technol.* **2014**, *267*, 289–301. [CrossRef]
18. Daraio, D.; Villoria, J.; Ingram, A.; Alexiadis, A.; Stitt, E.; Marigo, M. Investigating grinding media dynamics inside a vertical stirred mill using the discrete element method: Effect of impeller arm length. *Powder Technol.* **2020**, *364*, 1049–1061. [CrossRef]
19. Jin, X.; Wang, S.; Shen, Y. DEM study of the effect of impeller design on mixing performance in a U-shape ribbon mixer. *Adv. Powder Technol.* **2022**, *33*, 103334. [CrossRef]
20. Tsugeno, Y.; Sakai, M.; Yamazaki, S.; Nishinomiya, T. DEM simulation for optimal design of powder mixing in a ribbon mixer. *Adv. Powder Technol.* **2021**, *32*, 1735–1749. [CrossRef]
21. Chandratilleke, G.; Yu, A.; Stewart, R.; Bridgwater, J. Effects of blade rake angle and gap on particle mixing in a cylindrical mixer. *Powder Technol.* **2009**, *193*, 303–311. [CrossRef]
22. Boonkanokwong, V.; Remy, B.; Khinast, J.G.; Glasser, B.J. The effect of the number of impeller blades on granular flow in a bladed mixer. *Powder Technol.* **2016**, *302*, 333–349. [CrossRef]
23. Kloss, C.; Goniva, C. LIGGGHTS—Open Source Discrete Element Simulations of Granular Materials Based on Lammps. In *Supplemental Proceedings: Materials Fabrication, Properties, Characterization, and Modeling*; John Wiley & Sons, Inc.: Hoboken, NJ, USA, 2011; pp. 781–788. [CrossRef]
24. Pantaleev, S.; Yordanova, S.; Janda, A.; Marigo, M.; Ooi, J.Y. An experimentally validated DEM study of powder mixing in a paddle blade mixer. *Powder Technol.* **2017**, *311*, 287–302. [CrossRef]
25. Mio, H.; Higuchi, R.; Ishimaru, W.; Shimosaka, A.; Shirakawa, Y.; Hidaka, J. Effect of paddle rotational speed on particle mixing behavior in electrophotographic system by using parallel discrete element method. *Adv. Powder Technol.* **2009**, *20*, 406–415. [CrossRef]
26. Yaraghi, A. Mixing Assessment of Non-Cohesive Mono-Disperse and Bi-Disperse Particles in a Paddle Mixer—Experiments and Discrete Element Method (DEM). Master's Thesis, Ryerson University, Toronto, ON, Canada, 2018.
27. Hassanpour, A.; Tan, H.; Bayly, A.; Gopalkrishnan, P.; Ng, B.; Ghadiri, M. Analysis of particle motion in a paddle mixer using Discrete Element Method (DEM). *Powder Technol.* **2011**, *206*, 189–194. [CrossRef]
28. Jadidi, B.; Ebrahimi, M.; Ein-Mozaffari, F.; Lohi, A. Investigation of impacts of particle shape on mixing in a twin paddle blender using GPU-based DEM and experiments. *Powder Technol.* **2023**, *417*, 118259. [CrossRef]
29. Bhalode, P.; Ierapetritou, M. A review of existing mixing indices in solid-based continuous blending operations. *Powder Technol.* **2020**, *373*, 195–209. [CrossRef]
30. Alchikh-Sulaiman, B.; Ein-Mozaffari, F.; Lohi, A. Evaluation of poly-disperse solid particles mixing in a slant cone mixer using discrete element method. *Chem. Eng. Res. Des.* **2015**, *96*, 196–213. [CrossRef]
31. Palmer, J.; Reynolds, G.K.; Tahir, F.; Yadav, I.K.; Meehan, E.; Holman, J.; Bajwa, G. Mapping key process parameters to the performance of a continuous dry powder blender in a continuous direct compression system. *Powder Technol.* **2020**, *362*, 659–670. [CrossRef]
32. Sen, M.; Karkala, S.; Panikar, S.; Lyngberg, O.; Johnson, M.; Marchut, A.; Schäfer, E.; Ramachandran, R. Analyzing the Mixing Dynamics of an Industrial Batch Bin Blender via Discrete Element Modeling Method. *Processes* **2017**, *5*, 22. [CrossRef]
33. Gao, Y.; Muzzio, F.J.; Ierapetritou, M.G. Optimizing continuous powder mixing processes using periodic section modeling. *Chem. Eng. Sci.* **2012**, *80*, 70–80. [CrossRef]
34. Chandratilleke, G.; Dong, K.; Shen, Y. DEM study of the effect of blade-support spokes on mixing performance in a ribbon mixer. *Powder Technol.* **2018**, *326*, 123–136. [CrossRef]
35. Remy, B.; Glasser, B.J.; Khinast, J.G. The effect of mixer properties and fill level on granular flow in a bladed mixer. *AIChE J.* **2010**, *56*, 336–353. [CrossRef]
36. Goldhirsch, I. Introduction to granular temperature. *Powder Technol.* **2008**, *182*, 130–136. [CrossRef]
37. Remy, B.; Khinast, J.G.; Glasser, B.J. Discrete element simulation of free flowing grains in a four-bladed mixer. *AIChE J.* **2009**, *55*, 2035–2048. [CrossRef]
38. Ghotli, R.A.; Shah, R.S.S.R.E.; Raman, A. Effect of disc-blade intercepting angle on mixing performance in a multiphase stirred vessel. *Braz. J. Chem. Eng.* **2019**, *36*, 811–821. [CrossRef]

39. Zuo, Z.; Gong, S.; Xie, G. Numerical investigation of granular mixing in an intensive mixer: Effect of process and structural parameters on mixing performance and power consumption. *Chin. J. Chem. Eng.* **2021**, *32*, 241–252. [CrossRef]
40. Golshan, S.; Zarghami, R.; Norouzi, H.R.; Mostoufi, N. Granular mixing in nauta blenders. *Powder Technol.* **2017**, *305*, 279–288. [CrossRef]